



**HAL**  
open science

# The fibrous shell approach for the simulation of composite draping with a relevant orientation of the normals

R Bai, J Colmars, B Chen, N Naouar, P. Boisse

► **To cite this version:**

R Bai, J Colmars, B Chen, N Naouar, P. Boisse. The fibrous shell approach for the simulation of composite draping with a relevant orientation of the normals. *Composite Structures*, 2022, 285, 10.1016/j.compstruct.2022.115202 . hal-03543721

**HAL Id: hal-03543721**

**<https://hal.science/hal-03543721>**

Submitted on 26 Jan 2022

**HAL** is a multi-disciplinary open access archive for the deposit and dissemination of scientific research documents, whether they are published or not. The documents may come from teaching and research institutions in France or abroad, or from public or private research centers.

L'archive ouverte pluridisciplinaire **HAL**, est destinée au dépôt et à la diffusion de documents scientifiques de niveau recherche, publiés ou non, émanant des établissements d'enseignement et de recherche français ou étrangers, des laboratoires publics ou privés.



# The fibrous shell approach for the simulation of composite draping with a relevant orientation of the normals

R. Bai, J. Colmars, B. Chen, N. Naouar, P. Boisse\*

Université de Lyon, LaMCoS, CNRS, INSA-Lyon, F-69621, France

## ARTICLE INFO

### Keywords:

Fabrics/textiles  
Fibrous shell  
Forming  
Finite element analysis (FEA)

## ABSTRACT

Simulations of composite reinforcements draping use shell finite elements for which the bending behaviour is very particular. The fibrous composition of the reinforcements significantly reduces the bending stiffness compared to classical materials. Moreover, the kinematics of the deformation is strongly modified and does not follow classical theories such as Kirchhoff's. The objective of this paper is to show that a fibrous shell approach based on the quasi-inextensibility of the fibres makes it possible to correctly model the deformation during forming. In particular, the rotation of the material normal is simulated in good agreement with the forming experiments, which is not the case for the alternative approaches that have been proposed for the draping of composites.

## 1. Introduction

Manufacturing processes of composites are numerous and often complex. To avoid time-consuming and costly developments by trial and error, simulation of manufacturing processes is an interesting option. The forming of continuous fibre dry preforms and prepregs is a part of these processes for which simulation methods have been developed during the last decades [1–3]. The first approaches that have been developed (called pin-joined or fishnet algorithm) are geometrical methods based on the inextensibility of fibres [4–6]. These methods are very fast and are used in the design phases. However, these approaches do not consider the mechanical behaviour of the reinforcement nor the external forces during draping. Finite element forming simulations have been developed for the different scales of textile reinforcement. Although microscopic simulations (considering each fibre of the reinforcement) [7–10] and mesoscopic simulations (considering each yarn of the reinforcement) [11–13] have been developed, they require a significant numerical effort due to the large number of yarns and fibres of a textile reinforcement, which limits their use in practice. Most simulations of the forming (draping) of composite textile reinforcements are done at the macroscopic scale and consider the fibrous reinforcement as a continuous medium. This assumption is generally verified [1,14,15]. For some thick reinforcements, 3D finite element modelling has been performed. However, most of the reinforcements have a much smaller thickness than the other dimensions, and they are modelled by shells or

membranes. Because the bending stiffness of textile reinforcements is low, membrane type models (with zero bending stiffness) have been developed [16–19]. The membrane behaviour of textile reinforcements is specific with high tensile stiffnesses in the fibre directions and a low in-plane shear stiffness, but whose behaviour is important for the simulation of draping because the shear strains (change of angle between the warp and weft rovings) are large when forming on double curved surfaces [20–22]. Nevertheless, it has been shown that the bending stiffness plays a role in the forming of textile reinforcements, in particular with regard to the simulation of wrinkles [23–27]. Consequently, it is necessary to model the textile reinforcements by shells that integrate both the membrane behaviour specific to textiles and the bending behaviour. This last point is complex. Standard plate and shell theories (Kirchhoff, Mindlin) have been developed for classical continuous materials such as metals. In these approaches, the bending stiffness is fixed by the membrane stiffness and the plate thickness. Such an approach leads to a very overestimated bending stiffness for fibrous media. The low bending stiffness of textiles is due to the possible slippage between the fibres and is one of their main characteristics. This property is used for clothes that can be folded easily and also in the draping processes of composites that are performed with textile reinforcements or prepregs whose matrix is not cured.

To consider this specificity of textiles bending behaviour, several approaches have been proposed. The textile reinforcement can be seen as a laminate with several layers of various thickness and different

\* Corresponding author.

E-mail address: [philippe.boisse@insa-lyon.fr](mailto:philippe.boisse@insa-lyon.fr) (P. Boisse).

<https://doi.org/10.1016/j.compstruct.2022.115202>

Received 19 October 2021; Received in revised form 23 December 2021; Accepted 4 January 2022

Available online 10 January 2022

0263-8223/© 2022 The Authors.

Published by Elsevier Ltd.

This is an open access article under the CC BY-NC-ND license

(<http://creativecommons.org/licenses/by-nc-nd/4.0/>).

Young's modulus [28–30]. The characteristics of the different layers are chosen so that the effective membrane and bending properties are achieved. Another approach is to superimpose a finite element of membrane and a finite element of pure bending. The Young's modulus in the two elements is different. This provides the required low bending stiffness and large membrane stiffness [31–34]. Beam elements are used instead of shells in other approaches [35–38]. They are oriented in the direction of the warp and weft yarns and model tension and bending. Membrane elements are superimposed with only in-plane shear stiffness. Finally, stress resultant shells approaches make it possible to use independent behaviour laws between stress resultant and membrane deformations on the one hand and stress torque and bending on the other hand [39,40]. The different methods presented above make it possible to carry out simulations where the bending stiffness/membrane stiffness ratio corresponds to that of the analysed textile reinforcement. The deformed mid-surfaces obtained are correct. Nevertheless, these methods are often based on artificial assumptions that do not reflect the physics of deformation of the textile reinforcement. In addition, a major drawback is that the bending modelling is based on a classical theory. The material normals are the set of points attached to the material that are perpendicular to the mid-surface in the initial state. They are drawn on the beams in Fig. 1. This figure compares the rotation of material normals in a cantilever bending of two materials. One material is a classical continuous material (thick silica gel) (Fig. 1a), the other is a fibrous composite reinforcement (Fig. 1b).

Fig. 1a and b show that the rotations of the normals in the two cases are quite different. The rotation of the normals for the continuous material case (Fig. 1a) is consistent with standard shell theory and the normal remains perpendicular to the mid-surface after bending. This is not the case for fibrous materials (Fig. 1b) for which the deformation is driven by the quasi-inextensibility of the fibres with a possible local slip between the fibres. The approaches that have been presented above for modelling bending textile reinforcements all lead to a rotation of the material normal that remains perpendicular to the mid-surface which is erroneous. This point is important because the stresses in the fibres at a given position in the thickness depend on these rotations. The objective of this paper is to present an approach to model the draping of textile composite reinforcements and prepreps, called fibrous shell approach that leads to a deformation of the textile reinforcements with a relevant rotation of the material normals. These rotations are large during the forming processes. Bending tests and draping examples are compared with experiments, especially with respect to the orientation of normals.

## 2. Fibrous shell approach for textile reinforcement forming

The fibrous shell approach considers the two main specificities of fibrous reinforcements: the quasi-inextensibility of the fibres and the possible slippage between fibres. For this purpose, a particular form of internal virtual work  $\delta W_{int}$  is considered in the virtual work theorem:

$$\delta W_{ext} - \delta W_{int} = \delta W_{acc} \quad (1)$$

Here  $\delta W_{ext}$  is the exterior virtual work and  $\delta W_{acc}$  is the virtual work of

acceleration quantities. For a fibrous domain the virtual work of tension  $\delta W_{int}^{Ten}$  is:

$$\delta W_{int}^{Ten} = \sum_{f=1}^{N_{warp}} \int_{L'} T^{11f} \delta \epsilon_{11}^f dL + \sum_{f=1}^{N_{weft}} \int_{L'} T^{22f} \delta \epsilon_{22}^f dL \quad (2)$$

The superscript  $f$  indicates the fibre under consideration.  $T^{11f}$  and  $T^{22f}$  are the tensions in the fibre in warp and weft directions,  $N_{warp}$  and  $N_{weft}$  are the number of fibers in warp and weft directions.  $\delta \epsilon_{11}^f$  and  $\delta \epsilon_{22}^f$  are the virtual axial strains in the fibres in warp and weft directions. This form allows to integrate the quasi-inextensibility of the fibres because the tensions are linked to the deformations in their direction by a stiffness which is great compared to the other stiffnesses of the textile reinforcement. The quasi-inextensibility of the fibres is taken into account for all fibres through the thickness. This is a key point for the orientation of material normals.

The virtual bending work  $\delta W_{int}^{Bend}$  is:

$$\delta W_{int}^{Bend} = \sum_{f=1}^{N_{warp}} \int_{L'} M^{11f} \delta \chi_{11}^f dL + \sum_{f=1}^{N_{weft}} \int_{L'} M^{22f} \delta \chi_{22}^f dL \quad (3)$$

where  $M^{11f}$  and  $M^{22f}$  are the bending moment in the fibres in warp and weft directions,  $\delta \chi_{11}^f$  and  $\delta \chi_{22}^f$  are the virtual curvatures in the fibres in warp and weft direction. When draping on a double-curved surface, shear deformations play an important role. The virtual in-plane shear work  $\delta W_{int}^{Shear}$  is:

$$\delta W_{int}^{Shear} = \sum_{f=1}^{N_{fibres}} \int_{\Omega} M^{sf} \delta \gamma^f d\Omega \quad (4)$$

where  $M^{sf}$  is the in-plane shear moment,  $\delta \gamma$  is the virtual in-plane shear angle. The internal virtual work is the sum of the three virtual works of tension, bending and plane shear:

$$\delta W_{int} = \delta W_{int}^{Ten} + \delta W_{int}^{Bend} + \delta W_{int}^{Shear} \quad (5)$$

There is no virtual transverse shear work, which reflects the possible slippage between the fibres. Nevertheless, there is some friction between these fibres during relative sliding. These are taken into account in the virtual work of bending by using the bending stiffness of the textile reinforcement (which integrates these frictions) instead of the sum of the stiffnesses of the fibres in Eq. (3). Thus, bending deformations in agreement with experiments are obtained without complicating the approach [41].

To simulate large deformations of textile reinforcements and in particular draping processes, the particular form of internal virtual work (Eq. (2)–(5)) is integrated in degenerate shell finite elements. In this approach, 3D finite elements are degenerated into shells and the displacements of the points are obtained from those of the mean surface and the rotation of material normals which remain straight. This approach is one of the main ways to develop finite element shells [42–45]. It is based on material normal rotations but does not contain

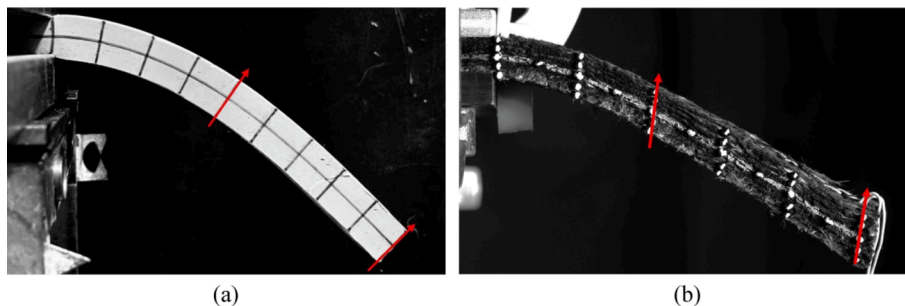


Fig. 1. Rotation of the material normal during a bending test. (a) Classical continuous material. (b) Fibrous material.

any Kirchhoff or Mindlin assumption. It is possible to integrate the particular form of the internal virtual works given Eq. (2)–(4). In the context of an explicit dynamics scheme, the displacement increment  $\Delta \mathbf{u} = {}^{i+1}\mathbf{x} - {}^i\mathbf{x}$  between time  ${}^i t$  and  ${}^{i+1} t$  is interpolated as follows in the case of a finite 3-node shell element (Fig. 2) [43,44]:

$$\Delta \mathbf{u}(\xi, \eta, \zeta) = \sum_{k=1}^3 N_k \Delta \mathbf{u}_k + \sum_{k=1}^3 N_k \frac{\zeta}{2} ({}^i h_m^k + \Delta h_m^k) (\Delta \alpha_k {}^i \mathbf{V}_1^k - \Delta \beta_k {}^i \mathbf{V}_2^k) + \sum_{k=1}^3 N_k \frac{\zeta}{2} \Delta h_m^k {}^i \mathbf{V}_m^k \quad (6)$$

Here  $\xi, \eta, \zeta$  are the material coordinates in the 3-node element.  $(\mathbf{V}_1^k, \mathbf{V}_2^k, \mathbf{V}_m^k)$  is a local orthogonal frame defined at each node  $k$  (Fig. 2).  $\mathbf{V}_m^k$  is the material normal at node  $k$ .  $N_k$  are the linear interpolation function of the three-node triangle.  $\Delta \mathbf{u}_k$  are the three increments of displacement degrees of freedom at node  $k$ ,  $\Delta \alpha_k$  and  $\Delta \beta_k$  are the two increments of rotation degrees of freedom at node  $k$ .  $h_m$  is the thickness in the direction of the pseudo normal. The thickness  $h$  in the direction  $\mathbf{n}_p$  perpendicular to the mean plane defined by the nodes ( $k = 1, 2, 3$ ) is the sum of the fibre thicknesses in this  $\mathbf{n}_p$  direction. This thickness  $h$  is assumed to be constant during the deformation. This assumption is verified experimentally, consequently:

$$h_m^k = \frac{h}{\mathbf{V}_m^k \cdot \mathbf{n}_p} \quad (7)$$

The kinematics Eq. (6) is used to calculate the increments of tension and in-plane shear strains as a function of the degrees of freedom of displacement and rotation in the whole shell. Regarding the curvatures, they are not connected to the rotation of the normals of the element. They are calculated from the position of the neighbouring elements (Fig. 2) following the method proposed for rotation free finite elements of shells with three nodes [46,47]. This way to calculate the curvatures is important in the present approach because for fibrous reinforcements, the curvature of the shell is not related to the position of the material normal (Fig. 1). The tensile, in-plane shear strains and curvatures being

function of the degrees of freedom of the element, the forms of the virtual works Eq. (2)–(5) give the nodal internal forces corresponding to the degrees of freedom of displacements and rotations [48,49].

### 3. Bending tests on textile reinforcement

#### 3.1. Presentation of the studied reinforcement

The G1151® fabric is based on an interlock weaving, three yarns are linked by the weaving in the thickness. The properties of the G1151® reinforcement are given in Table 1. The bending behaviour is measured from 3-point bending test and the in-plane shear behaviour is measured from bias-extension test [50]. Tensile and bending behaviour are assumed to be linear for simplicity, in-plane shear behaviour is non-linear.

#### 3.2. L-Flange forming

The L-Flange forming test is carried out on a stack of ten plies of parallel Hexcel G1151® reinforcement. The left end remains horizontal and is not tightened, allowing the sliding between the fibres meanwhile the displacement and the rotation of  $90^\circ$  are imposed at the right side (Fig. 3a) [51]. A bevel due to the quasi-inextensibility of the fibre and the deformed geometry is observed at the left end of specimen (Fig. 3b). The measured angle between the bevel direction and horizontal direction is  $32^\circ$ . A simulation using the proposed fibrous shell approach is shown in Fig. 3c. The simulated bevel angle is  $32.3^\circ$  which is in good agreement with experiment. Besides, the proposed shell approach uses only one element in the thickness. This considerably reduces the size of the numerical model used in [51] which is based on a stack of shell elements in contact and friction. The directions of the material normals in the experiment and obtained by simulation are compared in Fig. 3. They are in good agreement.

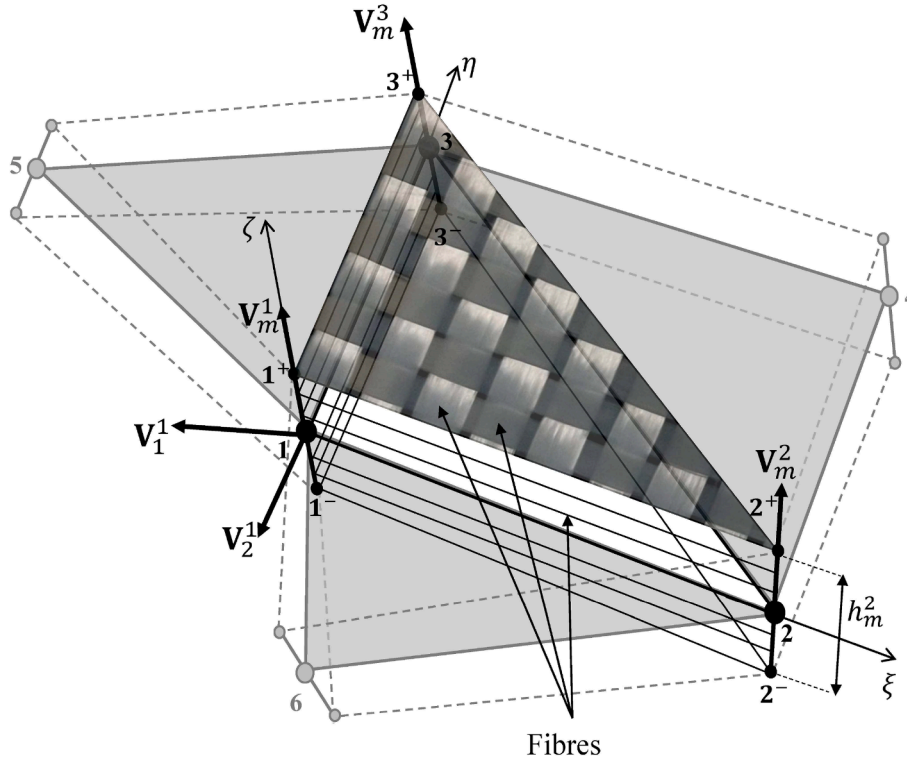
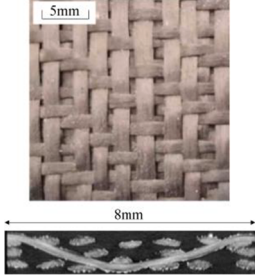
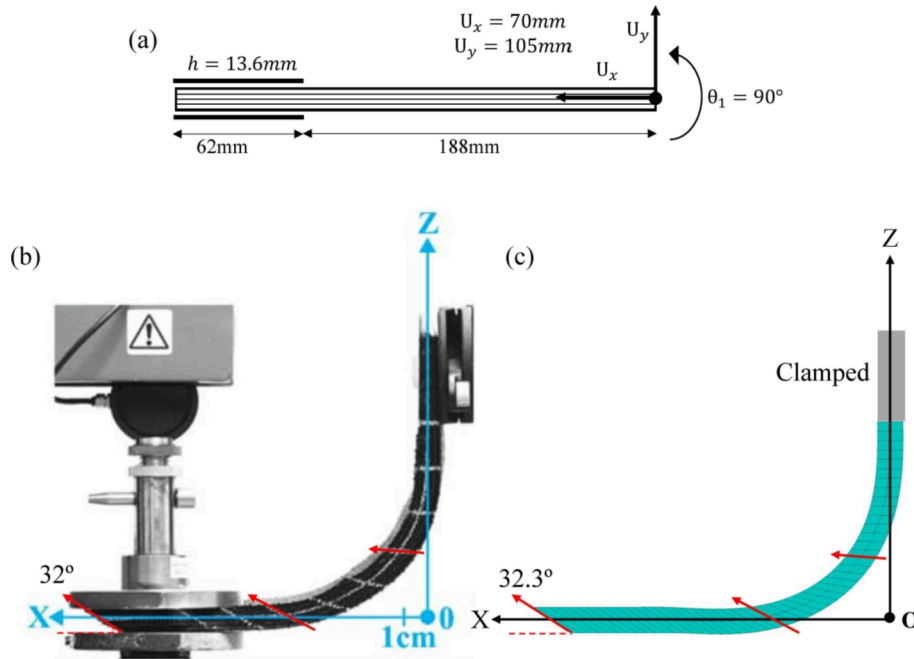


Fig. 2. Fibrous shell finite element.

**Table 1**  
Characteristics and mechanical property of G1151® reinforcement.

	Manufacturer fibres	Weave pattern		
	Hexcel carbon 6 K	Interlock (see the picture on the left)		
	Yarn density	Areal density	Single layer thickness	
	7.5 yarns/cm	630 g/ m <sup>2</sup>	1.3 mm	
Tensile	Bending	In-plane shear		
$T^{\alpha\alpha} = C_{\alpha}\epsilon_{\alpha\alpha}$ ( $\alpha = 1$ or $2$ ) $C_{\alpha} = 2300$ N/mm	$M^{\alpha\alpha} = B_{\alpha}\chi_{\alpha\alpha}$ ( $\alpha = 1$ or $2$ ) $B_{\alpha} = 6.5$ N mm	$M' = k_1^{\gamma} \gamma + k_3^{\gamma} \gamma^3 + k_5^{\gamma} \gamma^5 k_1^{\gamma} = 4.467E^{-2}$ N mm $k_3^{\gamma} = -4.425E^{-2}$ N mm $k_5^{\gamma} = 5.292E^{-2}$ N mm		



**Fig. 3.** L-Flange forming (a) Test conditions (b) Experiment, (c) Simulation.

**3.3. Thin specimen bending**

The objective of this test is to show that the bending of fibrous media does not tend towards the Kirchhoff solution when the thickness is very small and that the fibrous shell approach presented in this paper provides good orientation of the normals in this case.

The specimen consists of 20 sheets of paper as a substitute of the fibre layers (the properties are given in Table 2). Stacks of sheets of paper constitute a model fibrous material [41]. The thickness of the specimen is 2.3 mm which is small compared with the length of specimen which is 297 mm. The specimen is subjected to bending by imposing the rotations at the two ends. The right end was clamped, and the left end made possible slippage between fibres (Fig. 4).

The experimental deformed shape is shown in Fig. 5a, and the corresponding simulation using the proposed fibrous shell approach is displayed in Fig. 5b. Fig. 5c compares the experimental and numerical

rotations of the material normal and Fig. 5d compares the thickness along material normal direction. It can be seen that the normals do not remain perpendicular to the mid-surface and that their orientation is well simulated by the fibrous shells presented here.

**3.4. Bending with fibre orientation at ±45°**

In Fig. 6a, a stack of ten layers of G1151® oriented at ±45° is subjected to a bending with the two ends clamped [51]. In this bending test, the material normals remain perpendicular to the mid-surface (Fig. 6). This deformation corresponds to positive in-plane shear in the reinforcement in the upper part of specimen and negative in-plane shear in the bottom. Fig. 6 shows the angle between the warp and weft directions on the top and bottom of the specimen after bending. There is no fibre in the principal direction of the specimen and consequently no quasi-inextensibility condition.

The proposed fibrous shell is used to simulate this experiment condition. A single element in the thickness is used. The numerical result (Fig. 6b) is in good agreement with experiment. The in-plane shear angle for top and bottom layer and rotation of material director are correctly obtained by the simulation. In the experiment as in the simulation, the material normals remain perpendicular to the mid-surface of the specimen.

**Table 2**  
Properties of a single sheet of paper.

Areal density	Single layer thickness
80 g/m <sup>2</sup>	0.1 mm
Tensile stiffness	Bending stiffness
$C = 230$ N/mm	$B = 0.4$ N mm

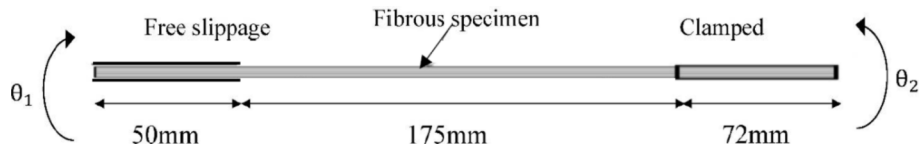


Fig. 4. Bending test of a thin fibrous material: Test conditions.

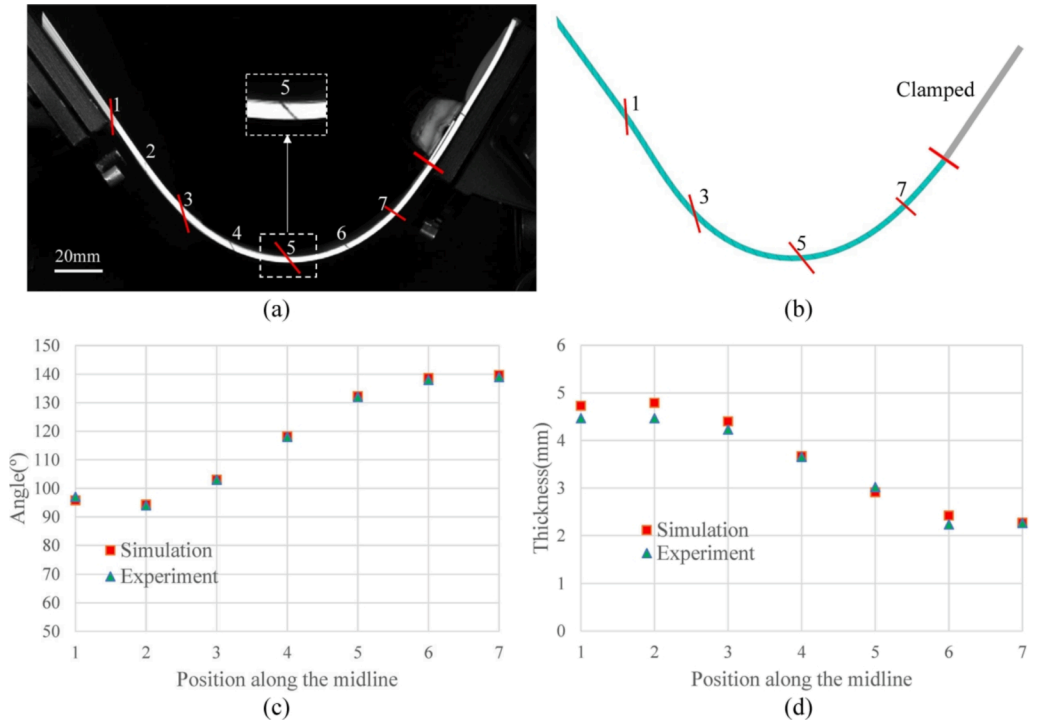


Fig. 5. Bending on a thin specimen (a) Experiment, (b) Simulation, (c) Angles between material normal and horizontal direction, (d) Thickness along material normal.

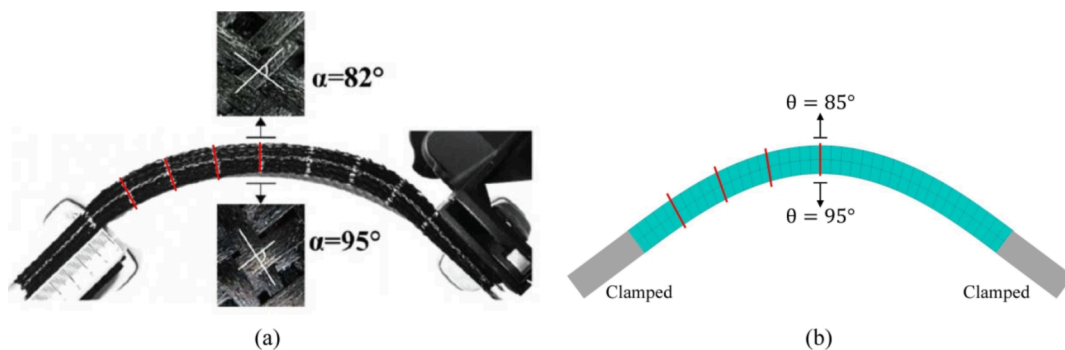


Fig. 6. Bending of a specimen with fibres oriented at  $\pm 45^\circ$  (a) Experiment, (b) Simulation.

#### 4. Composite reinforcements forming. Comparison between simulation and experiment

##### 4.1. Hemispherical forming

The hemispherical shape (Fig. 7) is the most commonly used double curved geometry to analyse the forming of textile composite reinforcements [52–61].

A universal testing machine is used to quasi-statically impose the displacement of the punch. The die and blank holder are transparent and allow the cameras to capture the deformation of the upper and lower surfaces of the specimen (Fig. 8). In particular, the two cameras measure

the position of marker points that give the in-plane shear angle on the upper and lower surfaces of the reinforcement and also give the orientation of the material normals after forming by considering two marker points facing each other on the upper and lower surfaces. The direction of material normal is represented by the angle between material normal and horizontal direction.

The punch, the blank holder and the die were modelled as rigid bodies. Contact was modelled using forward increment Lagrange multipliers and applying the Coulomb friction model [48]. The friction coefficient was 0.2

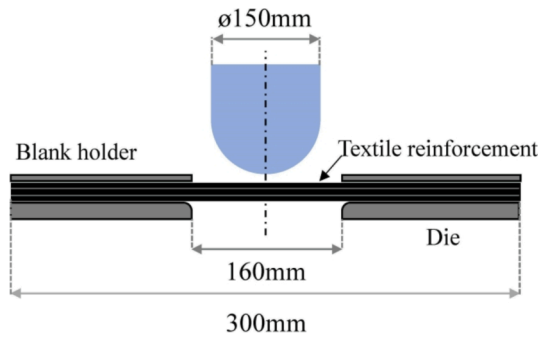


Fig. 7. Geometry of the tools of the hemispherical forming.

#### 4.1.1. Textile reinforcement oriented at 0–90°

The fabric blank is composed of four parallel plies of G1151 initially oriented at 0/90° (properties given in Table 1). The results of the simulation for the upper and lower surfaces are shown in Fig. 9a and b. Fig. 9c and d display the corresponding experimental results. No wrinkles were observed. The measured in-plane shear angles are obtained from the position of the neighboring marker points. They are in good agreement with the in-plane shear angle derived from the simulation. The shear angles on the upper and lower surface were close but slightly different.

**4.1.1.1. Analysis of the rotation of material normals.** Furthermore, the rotations of material normals were studied at specified positions. Fig. 10a shows the initial and deformed geometry of the specimen. The studied positions are initially positioned along the axis of symmetry and are marked from letter *a* to *e*. Along with the displacement imposed by the punch, the positions of the markers are changed but remain along the axis of symmetry. The opposed markers give the orientation of the material normals. Fig. 10b shows the deformed shape given by the simulation in the plane of symmetry where the position of the markers *a* to *e* is highlighted. Markers *a* and *b* remain in the plane. Markers *c*, *d*, *e* are located in the hemispheric part after forming. Moreover, analytical results can be obtained for the orientation of the normals based on the quasi-inextensibility of the fibres and the hemispherical shape of the punch (Fig. 10c).

Fig. 11a compares the experimental and numerical rotation angles of

the material normals. The correlation between the simulation and the experiment is good. At positions *a* and *b* situated in the die plane, there is no rotation of the material normal. At positions *c*, *d*, *e*, there is a significant rotation of the normal which is necessary to ensure the quasi-inextensibility of the fibres. Fig. 11b shows a good agreement between the rotations of the normals obtained in simulation, and by analytical calculation. This orientation of the normals is important because it determines the tensions in the fibres. In contrast to this correct orientation of the material normals after forming, which has been obtained here, all the alternative methods presented in the introduction of the article lead to normals that are perpendicular to the mid-surface and whose directions are therefore incorrect.

#### 4.1.2. Textile reinforcement oriented at ±45°

Fig. 12a show the position of the marker points. Points *a*, *b*, *c*, *d* are located on the axis of symmetry and thus no more in the direction of the fibres, consequently there is no inextensibility condition between them. The comparison of the orientation of the normals after forming is shown in Fig. 12b. They are in good agreement. Marker points *e*, *f*, *g*, *h* are situated along the fibre direction which is almost inextensible. Marker points *e* and *f* remains on the plane of the die, marker points *g* and *h* are in contact with the hemispherical punch after the draping. Orientations of the materials normal obtained by the simulation are in good agreement with experimental results (Fig. 12c).

#### 4.2. Forming with a tetrahedron tool

The tetrahedral geometry is of particular interest because it is the shape of the case corner parts [34,62–64]. It is a strongly double curved geometry.

##### 4.2.1. Textile reinforcement oriented at 0–90°

The geometry of the tools is given in Fig. 13. The fabric blank is composed of four parallel plies of G1151 initially oriented at 0/90° (properties given in Table 1). The comparison of the deformed shape obtained in the experiment and in the simulation are shown in Fig. 14. They are in good agreement. For simplicity reason, only the top layer is presented. There is no wrinkle detected in both the experiment and the simulation in all areas. The experimental deformed geometry shows several zones with quasi constant in-plane-shear. For zone 2 and 3, a change of in-plane shear angle is detected (From 0° to 30°). The

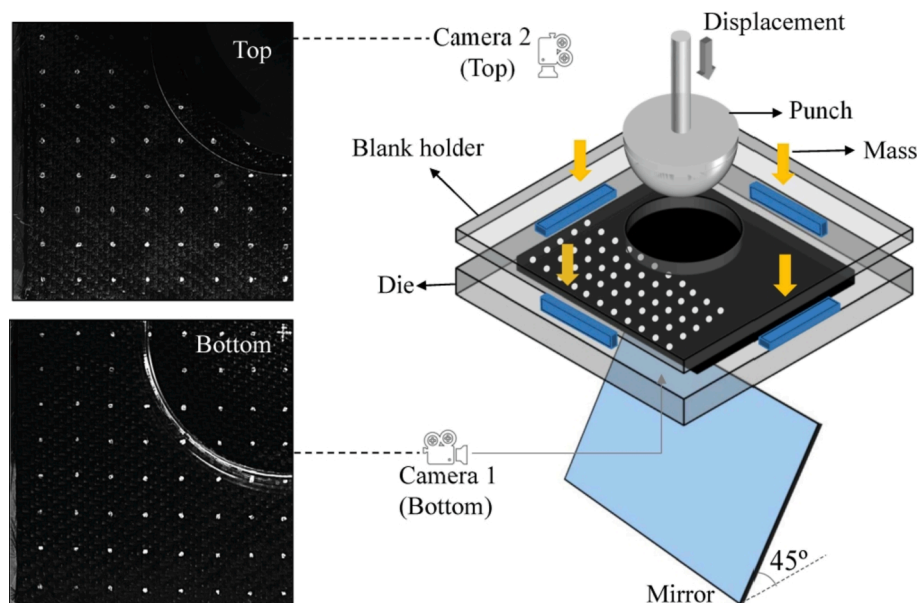
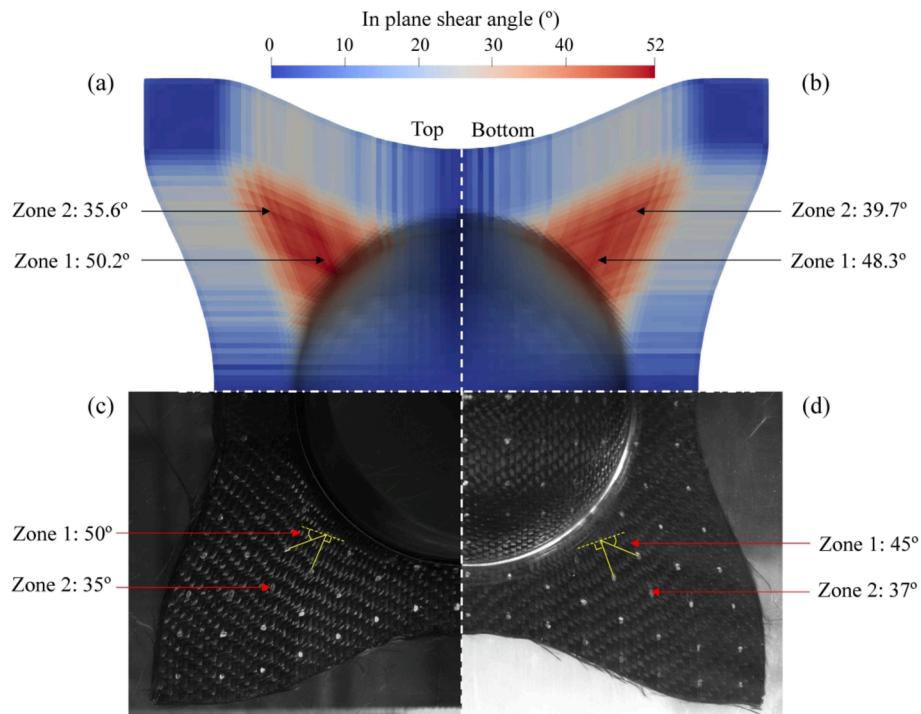
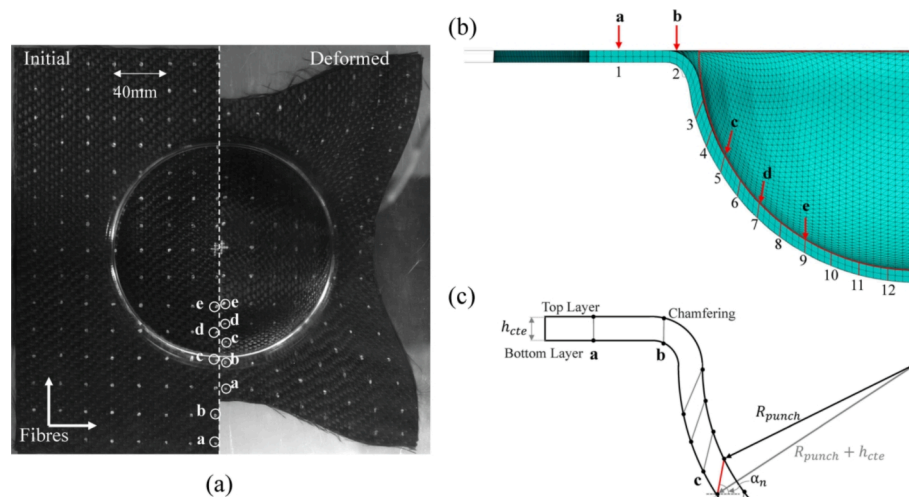


Fig. 8. Experimental device for material forming.



**Fig. 9.** Hemispherical forming of a textile reinforcement at 0°/90° and in-plane shear angle comparison: Simulation (a) Upper surface, (b) Bottom surface. Experiment (c) Upper surface, (d) Bottom surface.



**Fig. 10.** (a) Position of markers at initial and deformed configuration, (b) Numerical deformed configuration, (c) Theoretical analyse.

simulation well described this distribution of in-plane shear strains (From 0° to 31.8°) (Fig. 14). Other zones are also compared between simulation and experiment and show a good agreement.

4.2.1.1. *Analysis of the rotation of material normals.* Fig. 15a shows respectively the initial and deformed configuration. The marker points a-g are on the axis of symmetry and therefore along a direction of fibre. The marker points a-d situate in the tetrahedral zone after forming. Fig. 15b shows the comparison of the rotation angle of the material normals in experiment and simulation. They are in good agreement.

4.2.2. *Textile reinforcement oriented at ±45*

A tetrahedral forming of a textile reinforcement made of 4 plies of G1151 oriented at ±45° is shown in Fig. 16a. The marker points a-g are on the axis of symmetry, but they are no longer in the fibre direction. Consequently, the distance between each marking point is not fixed by the quasi-inextensibility of the fibres. After deformation, markers a and b situate in the tetrahedron zone. Other markers remain in the plane zone. The corresponding rotation angles obtained by the simulation are compared with experiment in Fig. 16b. The maximum difference between the experimental and numerical direction of material normal is



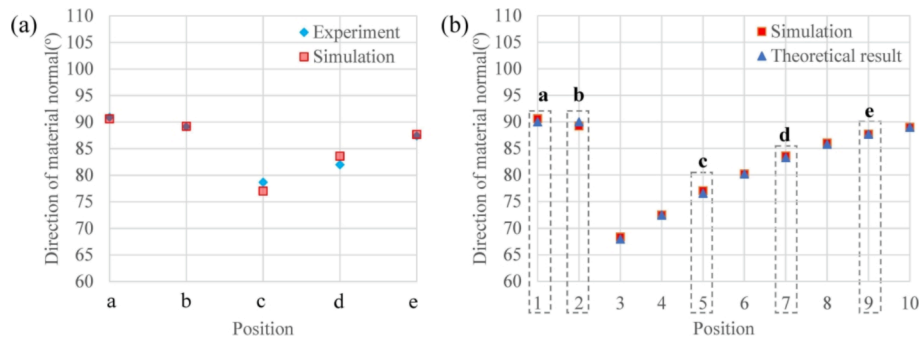


Fig. 11. Directions of the normals after forming:(a) Simulation versus Experiment, (b) Simulation versus Analyse.

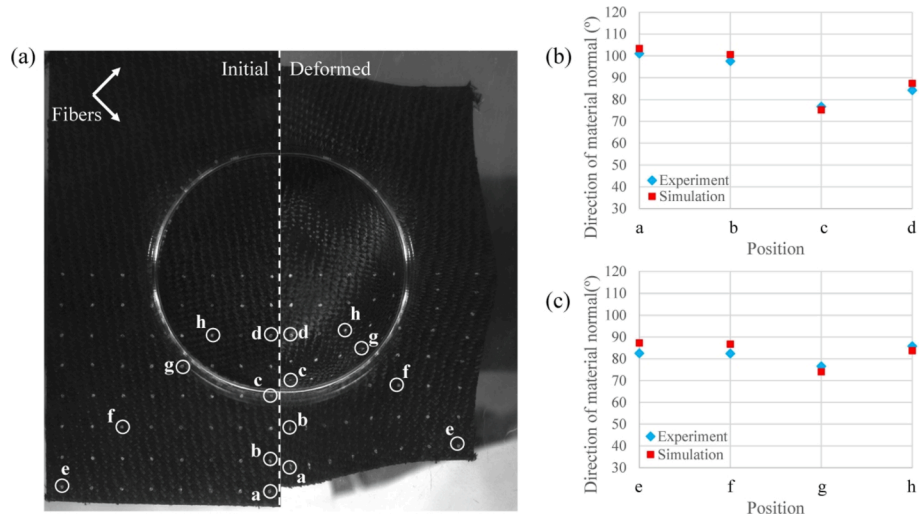


Fig. 12. Hemispherical forming of a textile reinforcement oriented at  $\pm 45^\circ$ : (a) Position of marker points in the initial and deformed configuration, Directions of the normals after forming: (b) on the axis of symmetry (c) in the fibre direction.

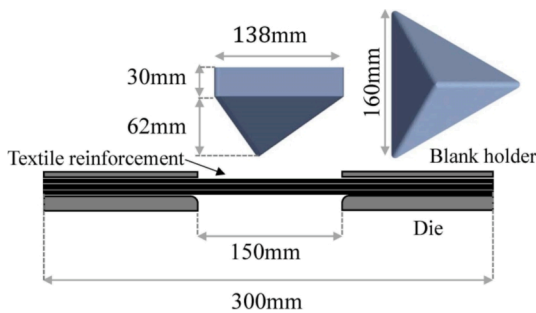


Fig. 13. Geometry of the tools of the tetrahedral forming.

less than 7%.

### 4.3. Hemispherical forming without blank holder

Wrinkling is one of the main defects that can develop during textile reinforcement draping. Their simulation is of great interest and is the subject of many studies [65–72]. To analyse the capability of the proposed fibrous shell approach to describe the development of wrinkles during forming, the hemispherical forming is performed without blank holder. The experimental deformed geometry is analysed by Digital Image Correlation (DIC). The DIC result is shown in Fig. 17a. Wrinkles develop along the symmetry axes x, y, and diagonal directions of the fabric. There are no wrinkles in the hemispherical zone.

The simulation using the proposed fibrous shell approach is

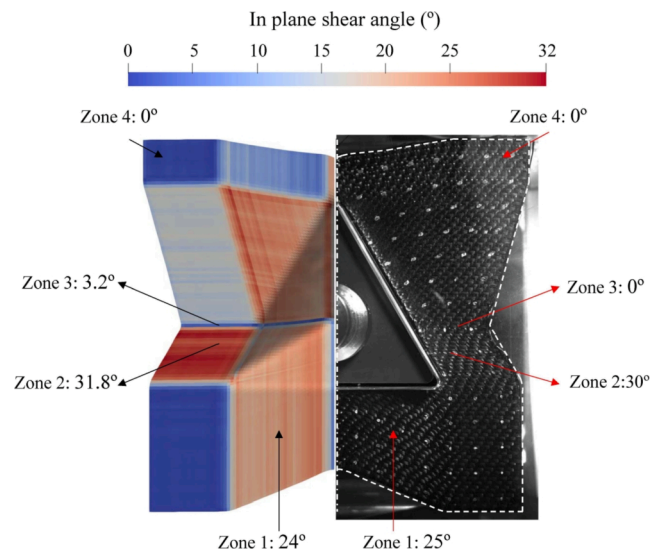
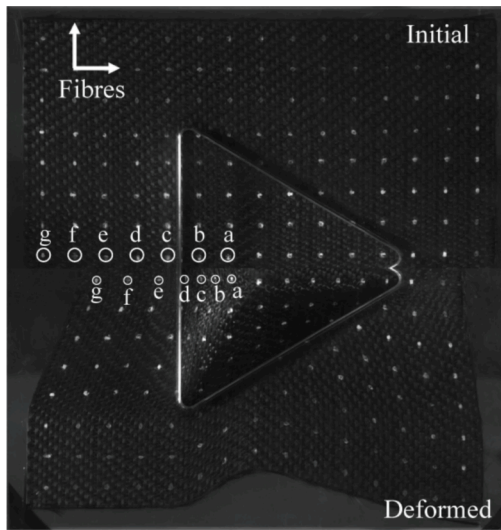
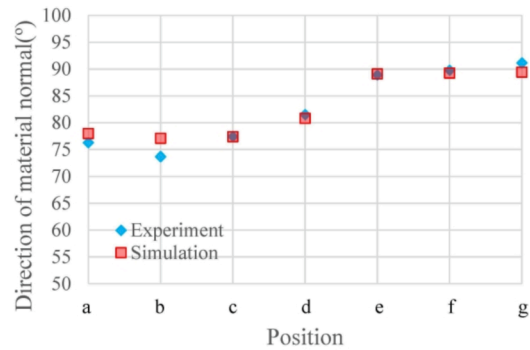


Fig. 14. Tetrahedron forming of a textile reinforcement at  $0^\circ/90^\circ$  and in-plane shear angle comparison: Simulation vs Experiment.

displayed in Fig. 17b, there is a fair correlation between experiment and simulation. The deformed geometry and the wrinkles are correctly described by the fibrous shell approach even if there is some difference between simulation and experiment.



(a)

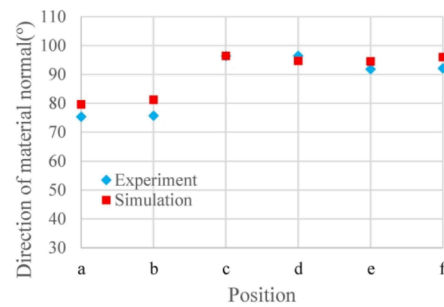


(b)

Fig. 15. Tetrahedron forming of a textile reinforcement at 0°/90°: (a) Position of marker points in the initial and deformed configuration (b) Comparison between the directions of the normals after forming obtained by experiment and by simulation.



(a)



(b)

Fig. 16. Tetrahedron forming of a textile reinforcement at ±45°: (a) Position of the marker points in the initial and deformed configuration; (b) Comparison between the directions of the normals after forming obtained by experiment and by simulation.

### 5. Conclusion

Simulation of textile reinforcement draping based on the proposed fibrous shell approach provides normal orientations consistent with forming experiments. This is not the case for the decoupling approaches that have been proposed previously which use the Kirchhoff assumption for the bending part. The fibrous shell approach is based on the effective physics of deformation of textile media. The quasi-inextensibility of the fibres at different positions in the thickness and the possibility of slippage between the fibres are the two main aspects that lead to a different kinematics of the deformation than in classical continuous materials. The material normals do not remain perpendicular to the mid-surface in most cases. This is important because the tensions in the fibers located at different positions in the thickness depend on the orientation of the material normals. Due to the high tensile stiffness of the fibers, a wrong orientation of the normals leads to tensile deformations and thus to high tensions in the fibers.

The fibrous shell approach presented in this paper may give rise to

some extension in future works. The transverse compaction of the fibrous reinforcement that can be generated by the forming tools can be taken into account. This compaction of the textile reinforcement take place in particular before resin injection in RTM processes and for the consolidation of composite parts made by thermoforming of thermoplastic prepregs. For this purpose, the fibrous shell approach must be integrated into solid-shell finite elements that have been developed recently and that consider the transverse deformation of the shell.

Another point concerns the forming of multi-layered textile composites. The fibrous shell approach proposed in this paper assumes that the fibres are oriented in single warp and weft directions. If the stack is composed of plies of different orientation, the forming is modified with slippage between plies. The extension of the fibrous shell approach to this case is one of the future development objectives.

#### CRediT authorship contribution statement

R. Bai: Investigation, Methodology, Software, Validation,

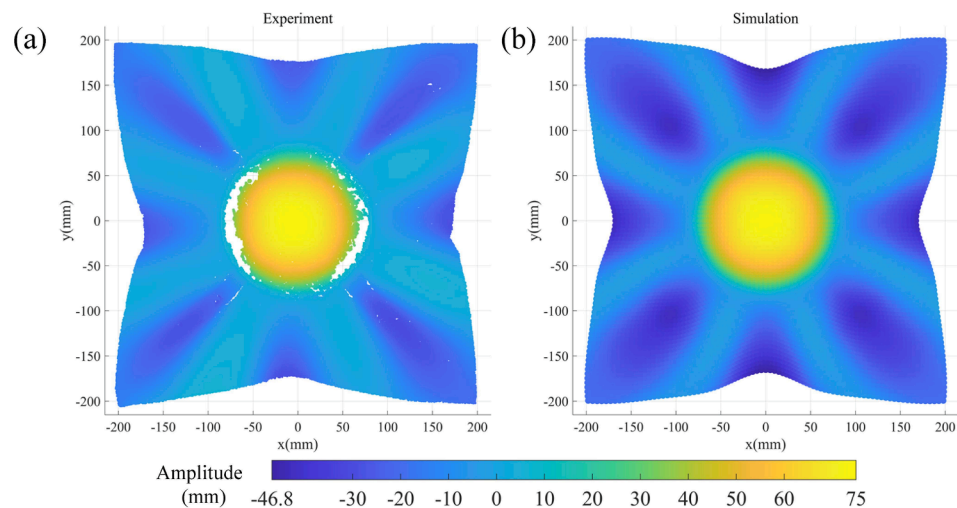


Fig. 17. Hemispherical forming without blank holder: (a) Experiment result (DIC), (b) Simulation result.

Visualization, Writing – original draft. **J. Colmars**: Investigation, Methodology, Supervision. **B. Chen**: Investigation, Methodology, Validation, Visualization. **N. Naouar**: Investigation, Software. **P. Boisse**: Conceptualization, Methodology, Supervision, Writing-review & editing.

#### Declaration of Competing Interest

The authors declare that they have no known competing financial interests or personal relationships that could have appeared to influence the work reported in this paper.

#### Acknowledgment

This work was supported by Agence Nationale de la Recherche, grant N° ANR-18-CE06-0011-04 AMOC.

#### References

- [1] Gereke T, Döbrich O, Hübner M, Cherif C. Experimental and computational composite textile reinforcement forming: A review. *Compos A Appl Sci Manuf* 2013;46:1–10.
- [2] Bussetta P, Correia N. Numerical forming of continuous fibre reinforced composite material: A review. *Compos A Appl Sci Manuf* 2018;113:12–31.
- [3] Liang B, Boisse P. A review of numerical analyses and experimental characterization methods for forming of textile reinforcements. *Chin J Aeronaut* 2021;34(8):143–63.
- [4] Long AC, Rudd CD. A simulation of reinforcement deformation during the production of preforms for liquid moulding processes. *Proc Inst Mech Eng, Part B: J Eng Manuf* 1994;208(4):269–78.
- [5] Potluri P, Perez Ciurezu DA, Ramgulum RB. Measurement of meso-scale shear deformations for modelling textile composites. *Compos A Appl Sci Manuf* 2006;37(2):303–14.
- [6] Hancock SG, Potter KD. The use of kinematic drape modelling to inform the hand lay-up of complex composite components using woven reinforcements. *Compos A Appl Sci Manuf* 2006;37(3):413–22.
- [7] Miao Y, Zhou E, Wang Y, Cheeseman BA. Mechanics of textile composites: Micro-geometry. *Compos Sci Technol* 2008;68(7-8):1671–8.
- [8] Durville D. Simulation of the mechanical behaviour of woven fabrics at the scale of fibers. *Int J Mater Form* 2010;3(S2):1241–51.
- [9] Latil P, Orgéas L, Geindreau C, Dumont PJJ, Rolland du Roscoat S. Towards the 3D in situ characterisation of deformation micro-mechanisms within a compressed bundle of fibres. *Compos Sci Technol* 2011;71(4):480–8.
- [10] Carvelli V, Fujii T, Okubo K. The effect of microfibrils cellulose modified epoxy on the quasi-static and fatigue behaviour of open hole carbon textile composites. *J Compos Mater* 2018;52(24):3365–80.
- [11] Creech G, Pickett AK. Meso-modelling of non-crimp fabric composites for coupled drape and failure analysis. *J Mater Sci* 2006;41(20):6725–36.
- [12] Gatouillat S, Bareggi A, Vidal-Sallé E, Boisse P. Meso modelling for composite preform shaping—simulation of the loss of cohesion of the woven fibre network. *Compos A Appl Sci Manuf* 2013;54:135–44.
- [13] Iwata A, Inoue T, Naouar N, Boisse P, Lomov SV. Coupled meso-macro simulation of woven fabric local deformation during draping. *Compos A Appl Sci Manuf* 2019;118:267–80.
- [14] Boisse P. *Finite element analysis of composite forming*. Woodhead Publishing; 2007. p. 46–79.
- [15] Boisse P, Hamila N, Madeo A. The difficulties in modeling the mechanical behavior of textile composite reinforcements with standard continuum mechanics of Cauchy. Some possible remedies. *Int J Solids Struct* 2018;154:55–65.
- [16] Yu W-R, Harrison P, Long A. Finite element forming simulation for non-crimp fabrics using a non-orthogonal constitutive equation. *Compos A Appl Sci Manuf* 2005;36(8):1079–93.
- [17] ten Thije RHW, Akkerman R, Huétink J. Large deformation simulation of anisotropic material using an updated Lagrangian finite element method. *Comput Methods Appl Mech Eng* 2007;196(33-34):3141–50.
- [18] Harrison P, Gomes R, Curado-Correia N. Press forming a 0/90 cross-ply advanced thermoplastic composite using the double-dome benchmark geometry. *Compos A Appl Sci Manuf* 2013;54:56–69.
- [19] Chen S, Harper LT, Endruweit A, Warrior NA. Formability optimisation of fabric preforms by controlling material draw-in through in-plane constraints. *Compos A Appl Sci Manuf* 2015;76:10–9.
- [20] Lebrun G, Bureau MN, Denault J. Evaluation of bias-extension and picture-frame test methods for the measurement of intraply shear properties of PP/glass commingled fabrics. *Compos Struct* 2003;61(4):341–52.
- [21] Lomov SV, Verpoest I. Model of shear of woven fabric and parametric description of shear resistance of glass woven reinforcements. *Compos Sci Technol* 2006;66(7-8):919–33.
- [22] Cao J, Akkerman R, Boisse P, Chen J, Cheng HS, De Graaf EF, et al. Characterization of mechanical behavior of woven fabrics: experimental methods and benchmark results. *Compos A Appl Sci Manuf* 2008;39(6):1037–53.
- [23] Boisse P, Hamila N, Vidal-Sallé E, Dumont F. Simulation of wrinkling during textile composite reinforcement forming. Influence of tensile, in-plane shear and bending stiffnesses. *Compos Sci Technol* 2011;71(5):683–92.
- [24] Syerko E, Comas-Cardona S, Binetruy C. Models of mechanical properties/behavior of dry fibrous materials at various scales in bending and tension: A review. *Compos A Appl Sci Manuf* 2012;43(8):1365–88.
- [25] Liang B, Hamila N, Peillon M, Boisse P. Analysis of thermoplastic prepreg bending stiffness during manufacturing and of its influence on wrinkling simulations. *Compos A Appl Sci Manuf* 2014;67:111–22.
- [26] Dangora LM, Mitchell CJ, Sherwood JA. Predictive model for the detection of out-of-plane defects formed during textile-composite manufacture. *Compos A Appl Sci Manuf* 2015;78:102–12.
- [27] Yu F, Chen S, Harper LT, Warrior NA. Simulating the effect of fabric bending stiffness on the wrinkling behaviour of biaxial fabrics during preforming. *Compos A Appl Sci Manuf* 2021;143:106308. <https://doi.org/10.1016/j.compositesa.2021.106308>.
- [28] Döbrich O, Gereke T, Diestel O, Krzywinski S, Cherif C. Decoupling the bending behavior and the membrane properties of finite shell elements for a correct description of the mechanical behavior of textiles with a laminate formulation. *J Ind Text* 2014;44(1):70–84.
- [29] Yu F, Chen S, Viisainen JV, Sutcliffe MPF, Harper LT, Warrior NA. A macroscale finite element approach for simulating the bending behaviour of biaxial fabrics. *Compos Sci Technol* 2020;191:108078. <https://doi.org/10.1016/j.compscitech.2020.108078>.
- [30] Han M-G, Chang S-H. Draping simulations of carbon/epoxy fabric prepreps using a non-orthogonal constitutive model considering bending behavior. *Compos A Appl Sci Manuf* 2021;148:106483. <https://doi.org/10.1016/j.compositesa.2021.106483>.

- [31] Haanappel SP, ten Thije RHW, Sachs U, Rietman B, Akkerman R. Formability analyses of uni-directional and textile reinforced thermoplastics. *Compos A Appl Sci Manuf* 2014;56:80–92.
- [32] Dörr D, Schirmaier FJ, Henning F, Kärger L. A viscoelastic approach for modeling bending behavior in finite element forming simulation of continuously fiber reinforced composites. *Compos A Appl Sci Manuf* 2017;94:113–23.
- [33] Dörr D, Henning F, Kärger L. Nonlinear hyperviscoelastic modelling of intra-ply deformation behaviour in finite element forming simulation of continuously fibre-reinforced thermoplastics. *Compos A Appl Sci Manuf* 2018;109:585–96.
- [34] Thompson AJ, Belnoue J-H, Hallett SR. Modelling defect formation in textiles during the double diaphragm forming process. *Compos B Eng* 2020;202:108357. <https://doi.org/10.1016/j.compositesb.2020.108357>.
- [35] Jauffrès D, Sherwood JA, Morris CD, Chen J. Discrete mesoscopic modeling for the simulation of woven-fabric reinforcement forming. *Int J Mater Form* 2010;3(S2):1205–16.
- [36] Mitchell CJ, Dangora LM, Sherwood JA. Investigation into a robust finite element model for composite materials. *Finite Elem Anal Des* 2016;115:1–8.
- [37] Harrison P. Modelling the forming mechanics of engineering fabrics using a mutually constrained pantographic beam and membrane mesh. *Compos A Appl Sci Manuf* 2016;81:145–57.
- [38] Giorgio I, Harrison P, Dell'Isola F, Alsayednoor J, Turco E. Wrinkling in engineering fabrics: a comparison between two different comprehensive modelling approaches. *Proc Roy Soc A: Math, Phys Eng Sci* 2018;474(2216):20180063.
- [39] Hamila N, Boisse P, Chatel S. Semi-discrete shell finite elements for textile composite forming simulation. *Int J Mater Form* 2009;2(S1):169–72.
- [40] Chen Bo, Colmars J, Naouar N, Boisse P. A hypoelastic stress resultant shell approach for simulations of textile composite reinforcement forming. *Compos A Appl Sci Manuf* 2021;149:106558. <https://doi.org/10.1016/j.compositesa.2021.106558>.
- [41] Liang B, Colmars J, Boisse P. A shell formulation for fibrous reinforcement forming simulations. *Compos A Appl Sci Manuf* 2017;100:81–96.
- [42] Ahmad S, Irons BM, Zienkiewicz OC. Analysis of thick and thin shell structures by curved finite elements. *Int J Numer Meth Eng* 1970;2(3):419–51.
- [43] Dvorkin EN, Bathe K-J. A continuum mechanics based four-node shell element for general non-linear analysis. *Eng Comput* 1984;1(1):77–88.
- [44] Huang HC, Hinton E. A new nine node degenerated shell element with enhanced membrane and shear interpolation. *Int J Numer Meth Eng* 1986;22(1):73–92.
- [45] Jayasankar S, Mahesh S, Narayanan S, Padmanabhan C. Dynamic analysis of layered composite shells using nine node degenerate shell elements. *J Sound Vib* 2007;299(1-2):1–11.
- [46] Onate E, Zárate F. Rotation-free triangular plate and shell elements. *Int J Numer Meth Eng* 2000;47(1-3):557–603.
- [47] Sabourin F, Brunet M. Detailed formulation of the rotation-free triangular element "S3" for general purpose shell analysis. *Eng Comput* 2006;23(5):469–502.
- [48] Hamila N, Boisse P, Sabourin F, Brunet M. A semi-discrete shell finite element for textile composite reinforcement forming simulation. *Int J Numer Meth Eng* 2009;79(12):1443–66.
- [49] Bai R, Colmars J, Naouar N, Boisse P. A specific 3D shell approach for textile composite reinforcements under large deformation. *Compos A Appl Sci Manuf* 2020;139:106135. <https://doi.org/10.1016/j.compositesa.2020.106135>.
- [50] Abdul Ghafour T, Colmars J, Boisse P. The importance of taking into account behavior irreversibilities when simulating the forming of textile composite reinforcements. *Compos A Appl Sci Manuf* 2019;127:105641. <https://doi.org/10.1016/j.compositesa.2019.105641>.
- [51] Huang J, Boisse P, Hamila N, Zhu Y. Simulation of wrinkling during bending of composite reinforcement laminates. *Materials* 2020;13(10):2374.
- [52] Cherouat A, Billoët JL. Mechanical and numerical modelling of composite manufacturing processes deep-drawing and laying-up of thin pre-impregnated woven fabrics. *J Mater Process Technol* 2001;118(1-3):460–71.
- [53] Cao J, Xue Pu, Peng X, Krishnan N. An approach in modeling the temperature effect in thermo-stamping of woven composites. *Compos Struct* 2003;61(4):413–20.
- [54] ten Thije RHW, Akkerman R. A multi-layer triangular membrane finite element for the forming simulation of laminated composites. *Compos A Appl Sci Manuf* 2009;40(6-7):739–53.
- [55] Peng X, Ding F. Validation of a non-orthogonal constitutive model for woven composite fabrics via hemispherical stamping simulation. *Compos A Appl Sci Manuf* 2011;42(4):400–7.
- [56] Duhovic M, Mitschang P, Bhattacharyya D. Modelling approach for the prediction of stitch influence during woven fabric draping. *Compos A Appl Sci Manuf* 2011;42(8):968–78.
- [57] Bel S, Boisse P, Dumont F. Analyses of the deformation mechanisms of non-crimp fabric composite reinforcements during preforming. *Appl Compos Mater* 2012;19(3-4):513–28.
- [58] Khan MA, Saleem W, Asad M, Ijaz H. A parametric sensitivity study on preforming simulations of woven composites using a hypoelastic computational model. *J Reinf Plast Compos* 2016;35(3):243–57.
- [59] Bardl G, Nocke A, Hübner M, Gereke T, Pooch M, Schulze M, et al. Analysis of the 3D draping behavior of carbon fiber non-crimp fabrics with eddy current technique. *Compos B Eng* 2018;132:49–60.
- [60] Allaoui S, Boisse P, Chatel S, Hamila N, Hivet G, Soulat D, et al. Textile composite structural analysis taking into account the forming process. *Compos B Eng* 2019;166:773–84.
- [61] Liu K, Zhang B, Xu X, Ye J. Experimental characterization and analysis of fiber orientations in hemispherical thermostamping for unidirectional thermoplastic composites. *Int J Mater Form* 2019;12(1):97–111.
- [62] Allaoui S, Boisse P, Chatel S, Hamila N, Hivet G, Soulat D, et al. Experimental and numerical analyses of textile reinforcement forming of a tetrahedral shape. *Compos A Appl Sci Manuf* 2011;42(6):612–22.
- [63] Allaoui S, Hivet G, Soulat D, Wendling A, Ouagne P, Chatel S. Experimental preforming of highly double curved shapes with a case corner using an interlock reinforcement. *Int J Mater Form* 2014;7(2):155–65.
- [64] Mathieu S, Hamila N, Bouillon F, Boisse P. Enhanced modeling of 3D composite preform deformations taking into account local fiber bending stiffness. *Compos Sci Technol* 2015;117:322–33.
- [65] Drapier S, Grandidier J-C, Potier-Ferry M. A structural approach of plastic microbuckling in long fibre composites: comparison with theoretical and experimental results. *Int J Solids Struct* 2001;38(22-23):3877–904.
- [66] Skordos AA, Monroy Aceves C, Sutcliffe MPF. A simplified rate dependent model of forming and wrinkling of pre-impregnated woven composites. *Compos A Appl Sci Manuf* 2007;38(5):1318–30.
- [67] Zhu B, Yu TX, Teng J, Tao XM. Theoretical modeling of large shear deformation and wrinkling of plain woven composite. *J Compos Mater* 2009;43(2):125–38.
- [68] Lightfoot JS, Wisnom MR, Potter K. A new mechanism for the formation of ply wrinkles due to shear between plies. *Compos A Appl Sci Manuf* 2013;49:139–47.
- [69] Hallander P, Akermo M, Mattei C, Petersson M, Nyman T. An experimental study of mechanisms behind wrinkle development during forming of composite laminates. *Compos A Appl Sci Manuf* 2013;50:54–64.
- [70] Farnand K, Zobeiry N, Poursartip A, Fernlund G. Micro-level mechanisms of fiber waviness and wrinkling during hot drape forming of unidirectional prepreg composites. *Compos A Appl Sci Manuf* 2017;103:168–77.
- [71] Belnoue JH, Nixon-Pearson OJ, Thompson AJ, Ivanov DS, Potter KD, Hallett SR. Consolidation-driven defect generation in thick composite parts. *J Manuf Sci Eng* 2018;140(7):071006.
- [72] Boisse P, Colmars J, Hamila N, Naouar N, Steer Q. Bending and wrinkling of composite fiber preforms and prepregs. A review and new developments in the draping simulations. *Compos B Eng* 2018;141:234–49.